3692 *Macromolecules* **2008**, *41*, 3692−3700

Effects of Bending and Torsional Potentials on High-Frequency Viscoelasticity of Dilute Polymer Solutions

Semant Jain* and Ronald G. Larson*

Department of Chemical Engineering, University of Michigan, Ann Arbor, Michigan 48109

Received October 22, 2007; Revised Manuscript Received February 3, 2008

ABSTRACT: To understand the mechanism of energy dissipation of dilute polymer solutions at high frequencies, we carry out a Brownian dynamics study of a linear polymer chain where beads represent individual backbone atoms and bending and torsional potentials are imposed to realistically model an alkane chain. We observe the end-to-end vector autocorrelation function from our simulations is in excellent agreement with the theoretical Rouse model predictions. Nevertheless, the backbone bond vector autocorrelation function exhibits a much slower decay than is predicted by the coarse-grain Rouse theory except near the longest relaxation time. We find that both the bending and torsional potentials slow down the contributions of local relaxation modes which brings the relaxation of short chains closer to single-exponential behavior than to the Rouse spectrum. This result is in qualitative agreement with measurements of birefringence relaxation (Lodge, T. P.; Miller, J. W.; Schrag, J. L. *J. Polym. Sci.: Polym. Phys. Ed.* **1982**, *20*, 1409−1425) and the notion of a "dynamical Kuhn length" (Larson, R. G. *Macromolecules* **2004**, *37*, 5110−5114).

1. Introduction

The slow dynamics of polymers in dilute solution are well described in the linear viscoelastic regime by the decades-old Rouse−Zimm theory[3,4] which coarse-grains a polymer chain into a sequence of frictional beads connected by Hookean (or linear) springs. Such a description is not expected to capture fast dynamics dominated by the local motions of one or a few backbone bonds since at long time scales such dynamics are expected to be subsumed into the effective bead drag coefficient and spring constant of the bead−spring chain. The success of this approach for slow dynamics has been demonstrated in numerous comparisons of the bead−spring model predictions to experimental data for long polymers in dilute solution[5] with the Gaussian behavior of the coil being gradually established[6−11] as the coil size increases.

Even so, what remains unresolved is the manner in which this coarse-grained bead−spring model breaks down at shorter time and distance scales than those for which linear "springs" can reasonably well capture the configurations of the chain. One might expect that at short times (or high frequencies) viscoelastic experiments would show indications of high-frequency modes that are controlled by motions of small groups of bonds that are influenced by bending and torsional potentials. Nevertheless, very surprisingly, experiments by Schrag, Lodge, and coworkers[1,12,13] have shown that the Rouse−Zimm bead−spring chain model can describe reasonably well the entire frequency range of dilute polystyrene or polyisoprene chains—even at frequencies high enough that single springs are expected to be strongly excited. This is true as long as the number of springs is chosen so that each spring represents a submolecule of molecular weight 4500 ± 500 for the case of polystyrene[5] and 2400 for polyisoprene[13] which in both cases corresponds to around 100 backbone bonds. In contrast, both experiments and simulations in melts show multiple "local" modes associated with relaxation of individual or small groups of bonds.[13−18] What is mysterious is why such modes do not appear in the viscoelastic measurements of dilute polymer solutions. Researchers[2,17] have suggested that torsional barriers to bond rotation might confer a large 'dynamic stiffness' to polymers that slows down modes requiring fast bond motion causing their relaxation to overlap with the terminal zone for short chains. This might occur only in dilute solutions but not in the melt because in the melt the diffusive motions of submolecules of the chain are slowed down by the high friction of the medium more than the local modes. As a result, in the melt (but not in dilute solution), the local rotational barriers can be surmounted faster than diffusive relaxation on longer length scales can occur and hence the relaxation of local modes can be temporally distinguished from the longer-range, diffusive, modes.

To test such ideas and to better understand the mechanism of energy dissipation at high frequencies in dilute solutions, one must study a polymer chain model that endows each short backbone bond with realistic bending and torsional angle restrictions.[2] Therefore, we conduct a Brownian dynamics study of a linear polymer chain in which the beads represent individual backbone atoms. We use stiff Fraenkel spring forces (which are harmonic with a zero force at a nonzero stretch)[19] to maintain the distance between atoms near 1.53 Å, bending forces to enforce tetrahedral bonding with a bending angle of 109° 47′, and torsional forces to create realistic barriers to torsional transitions. White noise is added to represent the Brownian force from the solvent. Overall, our model is similar to the united atom model of polyethylene. This enables us to compare the calculations of the end-to-end vector and individual bond (or unit spring) vector autocorrelation functions predicted by Brownian dynamics simulations using this model to the theoretical predictions of the coarse-grained Rouse model. In addition, we calculate the relaxation rates and amplitudes for all modes and compare our calculations to theoretical predictions and simulations for the melt state described in the literature. Finally, we also calculate the time-dependent scattering function, $S(q,t)$, from the model and discuss how these results compare to both to the Rouse−Zimm theory[3,4] and to the experimental data.

2. Simulations

2.1. Polymer Model. We model the polymer chain as a series of beads connected by stiff springs. If the position vector of the ith bead is denoted by $\mathbf{r}^i$, then the bond vector, $\mathbf{R}^i_S$, connecting the ith and $(i+1)$th beads is

$$\mathbf{R}^i_S = \mathbf{r}^{i+1} - \mathbf{r}^i \quad (1)$$

with the instantaneous bond length

---

* Corresponding author. E-mail: rlarson@umich.edu.

10.1021/ma702343w CCC: $40.75

$$l^i = |\mathbf{R}_S^i| = \sqrt{\sum_{k=1}^{3} (r_k^{i+1} - r_k^i)^2} \tag{2}$$

and

$$\mathbf{u}^i = \mathbf{R}_S^i / l^i \tag{3}$$

The ith bending angle formed made by the two adjacent bonds defined by beads i, $i + 1$, and $i + 2$ can be estimated by taking the vector products of the bonds connecting the beads:

$$\cos \theta_i = \frac{(\mathbf{r}^{i+2} - \mathbf{r}^{i+1}) \cdot (\mathbf{r}^i - \mathbf{r}^{i+1})}{l^{i+1} l^i} \tag{4}$$

The torsional angle, φ, formed by the two next-nearest neighbor bonds defined by the four adjacent beads i, j, k, and l is computed using[20]

$$\varphi = \mathrm{sign}(\varphi) \cos^{-1}(\mathbf{m} \cdot \mathbf{n}) \tag{5}$$

where

$$\mathbf{m} = \frac{\mathbf{r}^{ij} \times \mathbf{r}^{kj}}{|\mathbf{r}^{ij}||\mathbf{r}^{kj}|} \tag{6}$$

$$\mathbf{n} = \frac{\mathbf{r}^{kj} \times \mathbf{r}^{kl}}{|\mathbf{r}^{kj}||\mathbf{r}^{kl}|} \tag{7}$$

$$\mathrm{sign}(\varphi) = \text{sign of } [\mathbf{r}^{ij} \cdot (\mathbf{r}^{kj} \times \mathbf{r}^{kl})] \tag{8}$$

In the IUPAC notation,[21] in the cis conformation $\varphi = 0$ and all beads lie in a single plane with beads i and l on the same side of the line that passes through beads j and k. If one looks along the line connecting bead k toward bead j, if the bond connecting beads k and l must be rotated counterclockwise about the bond connecting k and j to reach the cis conformation via the smallest rotation angle, then the sign of φ is negative. This definition can be translated into notation more commonly used for polymers where $\varphi = 0$ corresponds to the trans conformation[20] through

$$\varphi(\text{polymer}) = \varphi(\text{IUPAC}) \pm \pi \tag{9}$$

2.2. Potential Energies. Since *n*-butane is the smallest chain that exhibits all bending and torsional conformations of a polymer chain, we use the Rychaert−Bellemans potential,[22,23] originally developed for *n*-butane, to describe the torsional potential energy of our model chain. The distance between adjacent C−C bonds is maintained near 1.53 Å by using a stiff Fraenkel stretching potential:

$$V_S^i(l^i) = \frac{\gamma_S}{2}(l^i - l_0)^2 \tag{10}$$

where γ_S is the stretching constant, l^i is the bond length of the ith bond, and l^0 is the equilibrium bond length. Similarly, the angles between adjacent bonds are maintained near the equilibrium bond angle, θ_0, which is 109° 47′ by use of the bending potential:

$$V_B^i(\theta_i) = \frac{\gamma_\theta}{2}(\cos \theta_i - \cos \theta_0)^2 \tag{11}$$

where γ_θ is the bending constant and θ_i is the angle formed by the ith and $(i + 1)$th bonds. To control the bond rotation about a central bond, we use the torsional potential:[22–24]

$$V_T^i(\varphi_i) = \gamma_\varphi \sum_{n=0}^{5} a_n \cos^n \varphi_i \tag{12}$$

where γ_φ is the torsional constant, φ_i is the torsional angle formed by the ith, $(i + 1)$th, and $(i + 2)$th bonds, and the a_n's are constants. This torsional potential yields four energy states: trans, gauche$^+$, gauche$^-$, and cis. The barrier to rotation between trans and gauche$^\pm$ states peaks at $\varphi = \pm 60°$. The potentials at various rotational angles are designated as V_T ($\varphi = 0°$) for the trans state which is the lowest energy state, V_{GT} ($\varphi = \pm 60°$) for the local maxima between trans and gauche states, V_G ($\varphi = \pm 120°$) for the gauche$^\pm$ states which are local energy minima, and V_C ($\varphi = \pm 180°$) for the cis state which is the maximum energy state. From the shape of the rotational potential, we can extract two additional relationships: $\partial V_T^i(\varphi_i)/\partial \varphi_i|_{\varphi = \pm 60°} = 0$ and $\partial V_T^i(\varphi_i)/\partial \varphi_i|_{\varphi = \pm 120°} = 0$. These six conditions enable us to relate the six rotational parameters, a_0, a_1, ..., a_5, to the known state potentials: $a_0 = [V_c + 8(V_{GT} + V_G)]/(18\gamma_\varphi)$, $a_1 = 14(V_{GT} - V_G)]/(9\gamma_\varphi) - V_C/(14\gamma_\varphi)$, $a_2 = -4[V_c - (V_{GT} + V_G)]/(9\gamma_\varphi)$, $a_3 = [8V_c - 99(V_{GT} - V_G)]/(18\gamma_\varphi)$, $a_4 = -2a_2$, and $a_5 = 8[-V_c + (V_{GT} - V_G)]/(9\gamma_\varphi)$.

In our simulations, the polymer is modeled as a phantom chain with no excluded volume interactions between atoms and with hydrodynamic interactions neglected. All friction is assumed to be concentrated at the atoms which are represented by beads and act as drag centers. Unlike Helfand et al.[24] who simulated cyclic chains (rings) to make all bonds equivalent, in our simulations of linear polymers the ends of the polymer chain are not connected. We do use their[24] values of stretching constant, $\gamma_S/m = 2.5 \times 10^{27}$ s^{-2}, and bending constant, $\gamma_\theta/m = 1.3 \times 10^7$ J/kg. The mass of the polymer bead, m, is 0.014 kg/mol. These constants are softened relative to physically realistic values to enable larger time steps to be taken during explicit numerical integration. The value of the torsional constant remains unchanged at $\gamma_\varphi/m = 6.6344 \times 10^5$ J/kg. All parameter values are summarized in Table 1.

2.3. Force Calculations. With the polymer chain immersed in solvent, the random motion of solvent molecules leads to Brownian forces acting on the chain, which can be represented by the form:[24,25]

$$\mathbf{F}_R^i = \sqrt{\frac{6\zeta k_B T}{\Delta t}}\mathbf{u} \tag{13}$$

where ζ is the bead frictional constant, k_B is the Boltzmann constant, T is the absolute temperature, Δt is the time step, and $\mathbf{u}$ is a vector whose each component has a uniform random distribution between −1 and 1. The temperature is set at 372 K for all the simulations in this work. To convert the stretching, bending, and torsional potentials to corresponding forces acting on the ith bead we use gradients of the potentials.

While the ideal length between two carbon bonds is 1.53 Å, if we use a realistic spring constant to keep the length fixed, the time step would have to be exceedingly small. When we soften the stretching potential's coefficient, γ_s/m, to one-seventh of its realistic value, the bond lengths are still within ±10% of the ideal length about 80% of the time and are within ±20% of the ideal length almost 100% of the time. Similarly, even with our bending potential's coefficient, γ_θ/m, reduced to one-fourth of its realistic value, the bending angles are within ±10° of the ideal value at 109° 47′ about 70% of the time and within ±20° of the ideal value almost 100% of the time. After neglecting inertial forces, to conserve momentum, the frictional force must be set equal to the sum of all the potential forces and the Brownian random force yielding[24]

$$\zeta \frac{\mathrm{d}\mathbf{r}^i}{\mathrm{d}t} = \mathbf{F}_S^i + \mathbf{F}_B^i + \mathbf{F}_T^i + \mathbf{F}_R^i \tag{14}$$

To validate the code, we use the energy conservation per time step approach which we have elaborated in Appendix 1.

2.4. Time Step Determination. Since we are only concerned with tracking the relaxation of chain configurations, we only need to pick a time step small enough for these properties to

Table 1. List of Parameters Used

	property	symbol	value	unit
1	frictional coefficient/mass	β	1×10^{14}	s^{-1}
2	bead mass	m	0.014	kg/mol
3	bead frictional coefficient	ζ	1.4×10^{12}	kg/(mol s)
4	equilibrium spring length	l_0	1.53×10^{-10}	m
5	equilibrium bending angle	θ_0	1090° 47′	degrees
6	torsional angle for trans state	φ_T	0	degrees
7	torsional angle for energy barrier	φ^*	±60	degrees
8	torsional angle for gauche state	φ_G	±120	degrees
9	torsional angle for cis state	φ_C	±180	degrees
10	stretching force coefficient/mass	γ_b/m	2.5×10^{27}	s^{-2}
11	bending force coefficient/mass	γ_θ/m	1.3×10^{7}	J/kg
12	rotational force coefficient/mass	γ_φ/m	6.634×10^{5}	J/kg
13	rotational force parameter	a_0	1	
14	rotational force parameter	a_1	1.3108	
15	rotational force parameter	a_2	−1.4135	
16	rotational force parameter	a_3	−0.3358	
17	rotational force parameter	a_4	2.8271	
18	rotational force parameter	a_5	−3.3885	
19	temperature	T	372	K
20	torsional potential for trans state	E_T	$0 = 0.000k_BT$	J/mol
21	torsional potential for gauche state	E_G	$2933 = 0.948k_BT$	J/mol
22	torsional potential for barrier	E^*	$12360 = 3.996k_BT$	J/mol
23	torsional potential for cis state	E_C	$44833 = 14.495k_BT$	J/mol

be accurate—even if the forces and potentials are not exact for individual atoms. Using the time step of $\Delta t = 5 \times 10^{-15}$ s chosen by Helfand and co-workers[24] as an upper limit using the softened potentials, we find no change in autocorrelation functions from the results obtained even when using a much smaller value $\Delta t = 10^{-16}$ s. Hence, to compute the autocorrelation functions, we use a time step of 5×10^{-15} s in our simulations.

3. Theory for Coil Expansion

A freely jointed chain (or bead−rod) model can be used to represent the coarse-grained equilibrium distribution of configurations of a realistic chain with bending and torsional potentials if the freely jointed chain has the same mean square end-to-end distance, $\langle R^2\rangle_0$, as the realistic chain, i.e., $\langle R^2\rangle_0 = N_K b_K^2$, where N_K is the number of Kuhn steps and b_K is the Kuhn step length of the freely jointed chain.[26,27] The "characteristic ratio" of a polymer is defined as the ratio of $\langle R^2\rangle_0$ of the actual polymer to that of an ideal chain in which each bond is freely jointed to neighboring bonds, for which $\langle R^2\rangle_0 = N_S l_0^2$, where N_S is the number of rodlike bonds and l_0 is the average bond length.[26] Thus, the characteristic ratio can be used as a measure of the coil expansion that results from the bending and torsional forces.

The contribution of the bending potential to the characteristic ratio is[28]

$$C_\infty^B = \frac{1 + \langle \cos \theta_C\rangle}{1 - \langle \cos \theta_C\rangle} \tag{15}$$

where $\theta_C \equiv \pi - \theta$ is the complement of the mean bending angle as defined in section 2.1. So, the mean square end-to-end distance of a chain with a bending potential becomes $\langle R^2\rangle_0 = C_\infty^B N_S l_0^2$. For tetrahedral bonding, $\langle \cos \theta_C\rangle = \cos \theta_C = 1/3$, yielding C_∞^B. Likewise the contribution of the torsional force to the characteristic ratio is[28]

$$C_\infty^T = \frac{1 + \langle \cos \varphi\rangle}{1 - \langle \cos \varphi\rangle} \tag{16}$$

where $\langle \cos \varphi\rangle$ is the average of the cosine of the torsional angle. When the trans/gauche barrier height is 0%, 100%, and 200% of the "base" barrier height, the corresponding characteristic ratio values, C_∞^T, are 2.9355, 2.4100, and 2.1461, respectively. Thus, the mean square end-to-end distance with bending and rotational forces becomes $\langle R^2\rangle_0 = C_\infty^T C_\infty^B N_S l_0^2$.

4. Results

The results presented in this section are obtained from simulations that are run for 10^{10} time steps with bead coordinates recorded 100% of the time for the first 10^4 steps, 10% of the time at regular intervals for time steps between 10^4 and 10^5, 1% of the time for time steps between 10^5 and 10^6, and so on, to conserve data storage while covering a very large dynamic range. The bead coordinates are then used to compute autocorrelation functions.

In order to study the behavior of the coil as a whole, we compute the end-to-end vector autocorrelation function:

$$\langle RR(s)\rangle|_{\mathrm{Sim}} \equiv \frac{\int_{t=0}^{t=D-s} \mathbf{R}(t+s)\cdot\mathbf{R}(t)\,\mathrm{d}t}{\int_{t=0}^{t=D-s} \mathbf{R}(t)\cdot\mathbf{R}(t)\,\mathrm{d}t} \tag{17}$$

where $\mathbf{R}(t) = \mathbf{r}^{N_s+1}(t) - \mathbf{r}^1(t)$, s is the autocorrelation time interval, and D is total simulation duration.

To analyze behavior at the level of individual Fraenkel springs, we compute the unit spring vector autocorrelation function:

$$\langle uu(s)\rangle|_{\mathrm{Sim}} \equiv \frac{\int_{t=0}^{t=D-s} \sum_{i=1}^{N_S} \mathbf{u}^i(t+s)\cdot\mathbf{u}^i(t)\,\mathrm{d}t}{\int_{t=0}^{t=D-s} \sum_{i=1}^{N_S} \mathbf{u}^i(t)\cdot\mathbf{u}^i(t)\,\mathrm{d}t} \tag{18}$$

We note that the unit spring vector autocorrelation function closely mimics the behavior of the mechanical stress relaxation function since bond orientational order is typically proportional to stress via the well-known stress-optic law.

To test the accuracy of our code, we compare the autocorrelation functions for a chain free of torsional and bending potentials but with a Hookean stretching force to the exact Rouse results for such chains. The Hookean spring law is given by[29]

$$\mathbf{F}_S^i = H\mathbf{R}_S^i \tag{19}$$

where

$$H = 2k_BT{\beta_S}^2 \tag{20}$$

$${\beta_S}^2 = \frac{3N_S}{2\langle R^2\rangle_0} = \frac{3}{2\langle R^2\rangle_{0,S}} = \frac{3}{2C_\infty^T C_\infty^B {l_0}^2} \tag{21}$$

using which we can calculate the autocorrelation function for the individual Hookean springs as

$$\langle R_S R_S(S)\rangle|_{sim} \equiv \frac{\int_{t=0}^{t=D-s} \sum_{i=l}^{N_s} \mathbf{R}_s^i(t+s)\cdot\mathbf{R}_s^i(t)\,\mathrm{d}t}{\int_{t=0}^{t=D-s} \sum_{i=l}^{N_s} \mathbf{R}_s^i(t)\cdot\mathbf{R}_s^i(t)\,\mathrm{d}t} \tag{22}$$

4.1. Theoretical Autocorrelation Predictions (Rouse Model). For the Rouse model (with Hookean springs and no bending or torsional barriers), the dynamics can be resolved into independent modes. The end-to-end vector, **R**, autocorrelation of the whole chain can be compared to the predictions of the Rouse model, yielding[26,30,31]

$$\langle RR(s)\rangle|_{\mathrm{Th}} \approx \frac{1}{\alpha}\sum_{p=1,3,5...}^{N_s} \frac{1}{p^2}\exp\left(-\frac{s}{\tau_p}\right) \tag{23}$$

where

$$\tau_p = \frac{\zeta}{8k_{\mathrm{B}}T\beta_{\mathrm{S}}^2 \sin^2[p\pi/2(N_{\mathrm{S}}+1)]} \tag{24}$$

with $\alpha = \sum_{p=1,3,5,...}^{N_S} 1/p^2$ and we set the mean square end-to-end distance of each spring equal to $3/2\beta_s^2 = \langle R^2\rangle_{0,\mathrm{S}} = C_\infty^{\mathrm{T}} C_\infty^{\mathrm{B}} l_0^2$, so that it matches that of a chain with stretching, bending, and torsional potentials.

Similarly, autocorrelation functions of the unit Fraenkel spring vectors and Hookean spring vectors can be compared to theoretical predictions using[30–32]

$$\langle uu(s)\rangle|_{\mathrm{Th}} \approx \frac{1}{N_{\mathrm{S}}}\sum_{p=1,2,3...}^{N_{\mathrm{S}}} \exp\left(-\frac{s}{\tau_p}\right) \tag{25}$$

and

$$\langle R_{\mathrm{S}} R_{\mathrm{S}}(s)\rangle|_{\mathrm{Th}} = \frac{1}{N_{\mathrm{S}}}\sum_{p=1,2,3...}^{N_{\mathrm{S}}} \exp\left(-\frac{s}{\tau_p}\right) \tag{26}$$

respectively, with eq 26 being an approximation valid at large s.

For Rouse chains (i.e., Hookean springs and no bending and torsional potentials) autocorrelation functions, $\langle RR(s)\rangle$ and $\langle R_{\mathrm{S}}R_{\mathrm{S}}(s)\rangle$, computed through simulations are in perfect agreement with the theoretical predictions for chains with 40 springs, $N_{\mathrm{S}} = 40$, and we also observe the -0.5 power-law region clearly appearing in the decay of $\langle R_{\mathrm{S}}R_{\mathrm{S}}(s)\rangle$. This further establishes the accuracy of our simulation code.

4.2. Stiff Spring Potential. Now, moving toward locally more resolved models, we first introduce the bond stretching force using the stiff Fraenkel spring potential. As is the case for Hookean springs, we observe excellent agreement of the predicted end-to-end vector autocorrelation function with that of the Rouse theory as can be seen in Figure 1.

While for Hookean springs there is nearly perfect agreement between simulations and theory for both the end-to-end vector and the spring vector autocorrelation functions, on introducing Fraenkel springs we observe modest differences between simulations and Rouse predictions of the spring vector autocorrelation function at times in the neighborhood of 10^{-12}–10^{-11} s in Figure 2. The modest discrepancy at short times is expected since this range of times corresponds to the rotational times of just one or a few bonds, which are too few to act as an effective Hookean spring. At longer times, $t > 10^{-11}$ s, the response is dominated by the collective motion of 5–10 or more bonds which is a sufficient number to act collectively as an effective Hookean spring. Hence, for $t > 10^{-11}$ s, there is good agreement between Rouse theory and simulations of chains with Fraenkel springs and no bending or torsional potentials.

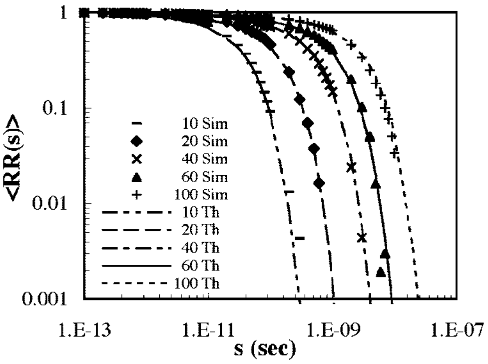

Figure 1. Comparison of simulated (Sim) and theoretical Rouse (Th) end-to-end vector autocorrelation function, $\langle RR(s)\rangle$, for $N_{\mathrm{S}} = 10$, 20, 40, 60, and 100 using Fraenkel springs with only Fraenkel stretching potential and no bending or torsional potentials.

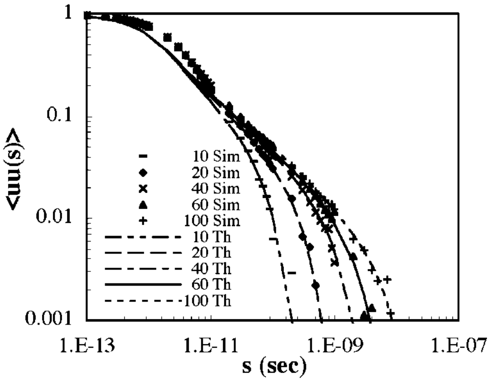

Figure 2. Same as Figure 1 except for unit spring vector autocorrelation function, $\langle uu(s)\rangle$.

4.3. Bending Angle Potential. Second, we add the bending force. Theoretically, the tetrahedral bonding angle is 109° 47′ ($\theta_{\mathrm{C}} = 70°\ 13'$) implying that $\cos\theta_{\mathrm{C}} = 0.3333$. Since we are using a softened coefficient for the bending potential, the distribution of bending angles is broadened relative to the "true" distribution. If we take into account this distribution in bending angles, from the simulation results, we obtain $\langle\cos\theta_{\mathrm{C}}\rangle = 0.3539$ which is within ~6% of the theoretical value for a fixed bending angle of 109° 47′. As is the case with stretching force only, when stretching and bending forces are both included, the simulated end-to-end vector autocorrelation function agrees increasingly well with the Rouse theory as the number of springs increases until nearly perfect agreement is obtained when N_{S} reaches 60 springs as can be seen in Figure 3. The relaxation of the end-to-end vector is dominated by the terminal relaxation process which can be deduced from the $1/p^2$ weighting of the modes in equation 23.

Figure 4 shows the unit spring vector autocorrelation function for $N_{\mathrm{S}} = 10$, 20, 60, and 100 springs. At short and intermediate times, the unit spring vector decays more slowly than in the Rouse predictions, although agreement is recovered in the terminal region which is expected since the simulated end-to-end vector relaxation $\langle RR(s)\rangle$ matches the Rouse predictions quite well as can be seen in Figure 3. Thus, unlike the effect of the fixed bond length which only influences the short time relaxation, the bond angle potential influences the relaxation, even for chains of 100 bonds out nearly to the terminal time. What is particularly interesting is that when $N_{\mathrm{S}} > 60$, $\langle uu(s)\rangle$ recovers the power-law time regime with slope similar to that of the Rouse theory but displaced to longer times. Eventually, at long times, the dynamics of the coil as a whole overshadow such local effects and hence the coil relaxation matches the Rouse prediction.

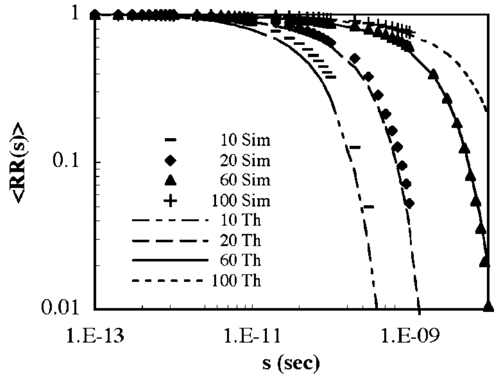

Figure 3. Comparison of simulated (Sim) and theoretical Rouse (Th) end-to-end vector autocorrelation function, $\langle RR(s)\rangle$, for $N_S = 10$, 20, 60, and 100 with Fraenkel stretching and bending potentials.

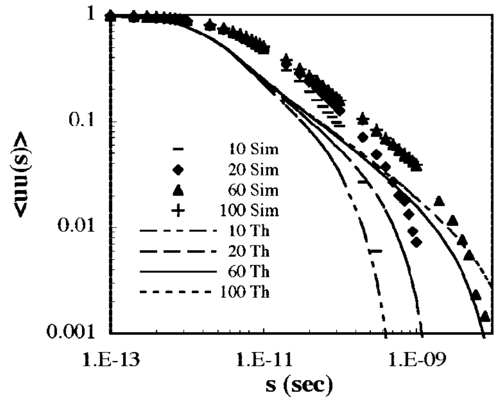

Figure 4. Same as Figure 3 except for unit spring vector autocorrelation function, $\langle uu(s)\rangle$.

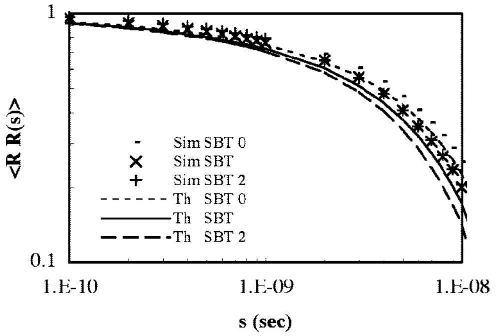

Figure 5. Comparison of simulated (Sim) and theoretical Rouse (Th) end-to-end vector autocorrelation function, $\langle RR(s)\rangle$, for $N_S = 60$ with barrier height between the trans and gauche ± states at 0% (SBT 0), 100% (SBT), and 200% (SBT 2) of the base height.

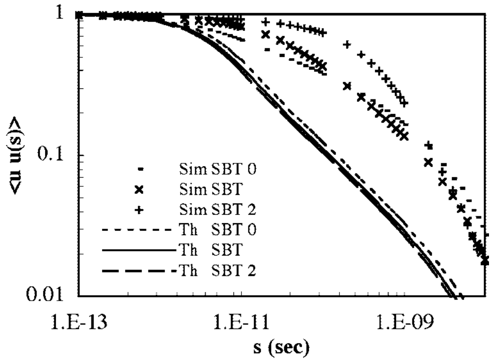

Figure 6. Same as Figure 5 except for unit spring vector autocorrelation function, $\langle uu(s)\rangle$.

4.4. Torsional Potential. We now examine the effect of the torsional potential by running the simulations at 0%, 100%, and 200% of the "base" barrier height of 12.36 kJ/mol between the trans and gauche states. When the barrier height is 0%, so that only the cis barrier exists, small deviations between the theoretical and simulated function $\langle RR(s)\rangle$ are apparent even for $N_S = 60$. Thus, the torsional force, even with no trans/gauche barrier, increases the coil stiffness which affects relaxation of the chain even on long length scales. This difference between theory and simulation increases with the rise in trans/gauche barrier height. While the effects are evident only for chains up to 60 springs in length for smaller barrier heights, we have seen (but do not present here) small deviations that creep in for even 100 springs at a barrier height of 200%. Additionally, as the barrier height increases, the average value of the cosine of the torsional angle, $\langle \cos \varphi\rangle$, decreases which reduces the torsional characteristic ratio, C_∞^{T}, showing that the coil shrinks slightly and leads to faster terminal relaxations. Figure 5 depicts the manner in which this is captured by simulations and the Rouse theory since we include C_∞^{T} in our calculation of the Rouse relaxation time spectrum as shown in eq 24.

Next, we identify the effect of changing the torsional barrier height on the bond (or unit spring) vector autocorrelation function. As soon as the cis barrier is introduced (with trans/gauche barrier absent), the power-law region completely disappears from the unit spring vector autocorrelation functions even for $N_S = 60$. The polymer relaxes far slower than is predicted by the Rouse model at both short and intermediate times and there is a rapid decay at long times. Thus, relaxation resembles that of a single spring (i.e., a single-exponential decay) more closely than that of a Rouse bead–spring chain. When the trans/gauche barrier is introduced at 100% of the base height, we observe reemergence of the power-law region when the number of springs increases to 60 or higher but this power-law region is greatly shifted to long times relative to the Rouse predictions. Still, for short chains ($N_S < 40$), the short- and intermediate-time behavior deviates noticeably from Rouse behavior. When the trans/gauche barrier increases to 200% of the base height, Figure 6 shows that even when a chain has 60 springs, the power-law region is not recovered. As is observed for the autocorrelation function for the end-to-end vector, Figure 6 shows the Rouse theoretical bond vector autocorrelation function relaxes marginally faster with increasing barrier height because of the slight chain contraction discussed above. All the same, simulations show that as the barrier height increases, relaxation is increasingly suppressed at short and intermediate times.

5. Discussion

We have found that the inclusion of bending and torsional potentials into a polymer chain model drastically alters the modes of polymer relaxation relative to the Rouse model. Even rather slow modes that involve coordinated motions of tens of bonds are affected although the terminal relaxation time is left nearly unchanged. We also find that the suppression or slowdown of internal modes becomes more severe as the torsional barrier separating trans and gauche states increases.

The suppression of internal modes is evidently a consequence both of the loss of configurational states produced by addition of bond angle constraints and of the slowing down of torsional transitions. This shifts the time scale of local modes toward the terminal time scale governing the relaxation of the molecule as a whole. The terminal mode is unshifted because it is governed mostly by pure rotational diffusion of the whole molecule. Even if internal degrees of freedom were completely frozen by imposing very high barriers to bond rotation, the chain as a whole could still rotate as a rigid object in the solvent and relax its end-to-end vector in a time comparable to that of a completely limp coil of the same radius.

Changing the bond stretching potential from Hookean to stiff Fraenkel, while keeping the overall chain dimension constant, has little effect on the relaxation spectrum except at short times. However, incorporation of a bending potential significantly slows the bond relaxation on both short and intermediate time scales. Presumably, the imposition of a strongly preferred bending angle makes complete relaxation, i.e., complete exploration of orientation space, of a given bond much more dependent on motion of other more distant bonds than is the case in the absence of a bending potential. Inclusion of a cis-torsional barrier further limits bond reorientation and additional imposition of a trans/gauche barrier not only shrinks the available conformational space but also slows even local sampling of that space.

5.1. Effect of Coarse Graining. Now, we examine the extent to which the behavior described above can be captured through standard coarse-graining approximations. Starting from a "realistic" polymer model with bending and torsional potentials, one can construct an "equivalent" freely jointed coarse-grained (CG) chain model with only stiff Fraenkel springs (and no bending or torsional potentials). Such a CG chain possesses the same mean square end-to-end vector, $\langle R^2\rangle_0$, as the realistic FG chain and has the same fully extended length, L, via the relationships

$$\langle R^2\rangle_0 = C_\infty n l^2 \tag{27}$$

$$L = 0.82nl = N_K b_K \tag{28}$$

where N_K is the number of bonds ("Kuhn steps") and b_K is the length of a CG bond (the "Kuhn length"). The factor of 0.82 arises from the zigzag configuration of the "fully extended length" of the FG chain which results from the tetrahedral bending angle. The above formulas allow us to obtain $N_K = 0.82^2 n/C_\infty$ and $b_K = C_\infty l/0.82$.

When bending and torsional potentials are absent $C_\infty = 1$ while imposition of a bending potential yields $C_\infty = C_\infty{}^B = 2$ and bending plus torsional potentials produces $C_\infty = C_\infty{}^B C_\infty{}^T = 5.8710$, 4.8200, and 4.2923 for 0%, 100%, and 200% trans/gauche barrier heights. The equivalent freely jointed chain model must have a reduced number of bonds, namely $N_K = 0.82^2 n/C_\infty$ and a longer bond length, namely $b_K = C_\infty l/0.82$, i.e., longer but fewer CG bonds, relative to the FG model. In addition, since the equivalent freely jointed chain has fewer beads than the original realistic chain, to reproduce the same total frictional drag, $\zeta_T|_0$, the drag coefficient on each bead in the CG chain needs to be increased so that the product of the number of beads and the bead drag coefficient remains the same as in the original chain, i.e., $\zeta_T|_{CG} = \zeta_T|_0 \Rightarrow \zeta|_{CG} = \zeta|_0(N_S + 1)|_0/(N_S + 1)|_{CG}$. Equivalently, we can simply multiply the time axis of the CG simulation by the ratio $(N_S + 1)|_0/(N_S + 1)|_{CG}$, where $(N_S + 1)|_{CG}$ is the number of beads in the CG chain and $(N_S + 1)|_0$ is the number of beads in the original chain.

First, we compare the autocorrelation functions computed through our simulations for a 60-bond chain with bending potential to those for an equivalent coarse-grained chain having only 20 stiff Fraenkel springs i.e., 20 CG bonds ($N_K = 0.82^2 n/C_\infty = 0.336 N_S = 20$) with each bond being 3.7317 Å long. We find that the end-to-end vector autocorrelation function $\langle RR(s)\rangle$ for the coarse-grained simulation with 20 freely jointed bonds perfectly matches that of the FG simulation of a chain with 60 bonds that has a bending potential. This implies that a coarse-grained model that uses only stiff springs is able to capture the end-to-end vector relaxation of a realistic chain with a bending potential. However, for the autocorrelation function of individual springs, $\langle uu(s)\rangle$, the CG model shows a slower relaxation on intermediate time scales than the simulations using 60 realistic bonds. Thus, except in the terminal region, the coarse-grained model is unable to capture the intermediate-scale dynamics of chains with a bending potential.

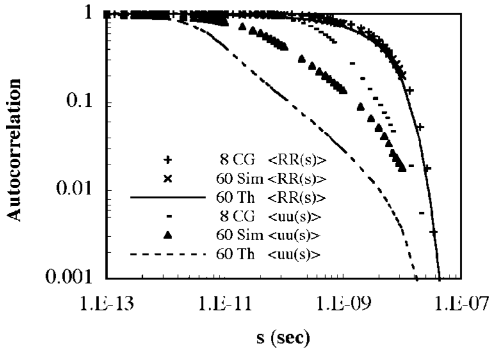

Figure 7. Comparison of fine grain simulated (Sim) and theoretical Rouse (Th) autocorrelation functions, $\langle RR(s)\rangle$ and $\langle uu(s)\rangle$, using 60 Fraenkel springs with stretching, bending, and torsional potential at 100% trans/gauche barrier height to corresponding results using eight coarse-grained (CG) bonds of bond length 8.9934 Å. Symbol × is not visible as it is overlapped for the most part by +.

Similarly, a coarse-grained chain "equivalent" to a 60-bond chain with both bending and torsional potentials has $N_K = 6$ or 7 bonds of length $b_K = 10.9544$ Å when the trans/gauche barrier height is 0%, $N_K = 8$ or 9 and $b_K = 8.9934$ Å when the trans/gauche barrier height is 100%, and $N_K = 9$ or 10 and $b_K = 8.0088$ Å when the trans/gauche barrier height is 200%. With increasing the trans/gauche barrier height (0%, 100%, and 200%), the difference between simulation results and CG predictions narrows significantly. Figure 7 shows the comparison between simulation and theoretical Rouse model with a 100% trans/gauche barrier. We find that the CG predictions match the realistic fine grain simulations better with increasing barrier height with very little difference remaining between the two at a 200% trans/gauche barrier height (data not shown).

5.2. Torsional Bond Relaxation Rate. Fixman[17] carried out a simulation of a simplified polymer model with 90° bending angle and three torsional barriers which showed suppression of fast and intermediate time scale relaxation processes. We apply his approach to our more realistic simulations by fitting the normal mode relaxation rates for different models—stretching force only, stretching and bending forces, and stretching, bending, and torsional forces with different trans/gauche barrier heights—to a single exponential having a prefactor c_F^k and relaxation rate ν_F^k for each mode k. As expected, we find that a single exponential provides a very good fit to each of the normal mode relaxation functions. The normal mode relations are computed as follows:

$$\langle q_k q_k(s)\rangle \equiv \frac{\int_{t=0}^{t=D-s} \mathbf{q}_k(t)\cdot\mathbf{q}_k(t+s)\,\mathrm{d}t}{\int_{t=0}^{t=D-s} \mathbf{q}_k(t)\cdot\mathbf{q}_k(t)\,\mathrm{d}t} = c_F^k \exp\left(-\nu_F^k s\right) \tag{29}$$

where

$$\mathbf{q}_k = \sum_{i=1}^{i=N_S} Q_{ki}\mathbf{R}_S^i \tag{30}$$

$$Q_{ki} = \sqrt{\frac{2}{N_S+1}}\sin\left(\frac{\pi k i}{N_S+1}\right) \tag{31}$$

The modal relaxation rates are given in Figure 8 which also show a pattern similar to Fixman's[17] observations.

Next, we compute the amplitudes of the above modes computed for a chain in dilute solution using[33]

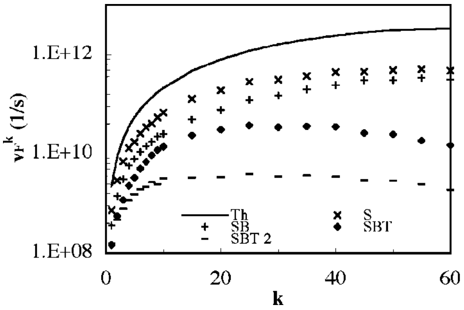

Figure 8. Bond relaxation rate, $\nu_F{}^k$, at different mode numbers, k, using Fixman's correlation for 60 springs with just the stretching force (S), stretching and bending forces (SB), and stretching, bending, and torsional forces with barrier heights of 100% (SBT) and 200% (SBT 2) of base height.

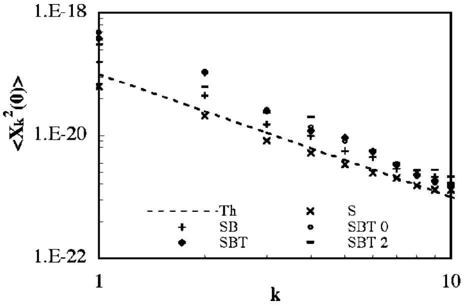

Figure 9. Amplitude of the bond relaxation for 60 springs with just the stretching force (S), stretching and bending forces (SB), and stretching, bending, and torsional forces with the trans/gauche barrier heights of 0% (SBT 0), 100% (SBT), and 200% (SBT 2) of base height. Dashed line indicates the k^{-2} scaling expected from Rouse theory (Th).

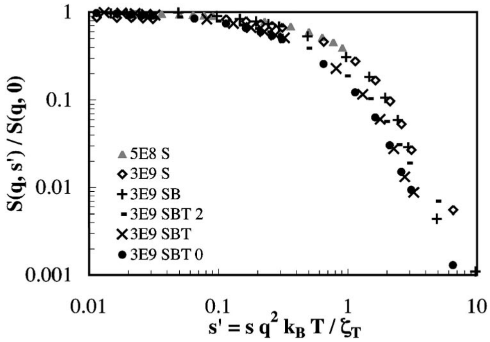

Figure 10. Structure factor calculations for dilute polymer chains when $N_S = 60$ with just the stretching force (S), stretching and bending forces (SB), and stretching, bending and torsional forces with the trans/gauche barrier height at 0% (SBT 0), 100% (SBT), and 200% (SBT 2) of the base height when the wavenumber, q, is $q = 5 \times 10^8$ m^{-1} (5E8) and $q = 3 \times 10^9$ m^{-1} (3E9).

$$\langle X_k X_k(s)\rangle \equiv \int_{t=0}^{t=D-s} \overline{X_k}(t)\cdot\overline{X_k}(t+s)\,\mathrm{d}t = c_K^k \exp\left(-\nu_K^k s\right) \quad (32)$$

where

$$\overline{X_k}(t) = \frac{1}{N_S+1}\sum_{i=1}^{i=N_S+1} \cos\left(\frac{\pi k(i-0.5)}{N_S+1}\right)\mathbf{r}_i(t) \quad (33)$$

To check our calculations, we compare our results of $\langle(\mathbf{X}_1(0))^2\rangle$ to the theoretical[33] scaling $\langle(\mathbf{X}_1(0))^2\rangle \approx \langle R^2\rangle_0/2\pi^2$, where $\mathbf{R}$ is the end-to-end vector of the chain, and find our results are in good agreement. Our calculations shown in Figure 9 indicate that the amplitude of relaxation decays in the range of k^{-1} to k^{-2} close to k^{-2} expected from the Rouse theory[33,34] but in contrast to melts where decay rate changes from k^{-2} for slower relaxation modes to k^{-3} for faster modes.[33]

5.3. Structure Function. The dynamics of polymers in dilute solution can be probed not only by linear viscoelastic measurements but also by measurements of dynamic scattering functions such as those obtained by neutron spin–echo experiments.[35] These experiments have shown that in dilute solution the dynamic structure factor closely follows the standard dilute solution theory of Zimm.[4] The Zimm theory, while being based on a coarse-grained bead–spring chain just like the Rouse theory, differs from the Rouse theory by its additional inclusion of hydrodynamic interactions. Hence, based on our simulations, one might have expected to see in the experiments large deviations from the Zimm theory in the dynamic structure factor at large values of the scattering wavenumber, q. However, such deviations were not seen.[35] To investigate further, we calculate the scattering function, $S(q,s)$, in the dilute region using[36]

$$S(\mathbf{q}, s) = \frac{1}{N_S}\sum_{i,j=1}^{i,j=N_S} \exp\left[i\mathbf{q}\cdot\left\{\mathbf{R}_i^S(t+s) - \mathbf{R}_i^S(t)\right\}\right] \quad (34)$$

which can be simplified for the case of a single chain in dilute solution as[37]

$$S(q,s) = \begin{cases} 1 + 4\pi\displaystyle\int_{r=0}^{r=\infty} r^2 g(r,s)\frac{\sin(qr)}{qr}\,\mathrm{d}r \\ \approx 1 + 4\pi\displaystyle\sum_{i=0}^{i=\infty} r_i^2 g(r_i,s)\frac{\sin(qr_i)}{qr_i}\Delta r, & s=0 \\ 4\pi\displaystyle\int_{r=0}^{r=\infty} r^2 g(r,s)\frac{\sin(qr)}{qr}\,\mathrm{d}r \\ \approx 4\pi\displaystyle\sum_{i=0}^{i=\infty} r_i^2 g(r_i,s)\frac{\sin(qr_i)}{qr_i}\Delta r, & s\neq 0 \end{cases} \quad (35)$$

Here, r_i is equal to $i\Delta r$ and $g(r,s)$ is the radial distribution function of the spring length which is computed as[37,38]

$$g(r,s) = \begin{cases} \dfrac{\displaystyle\int_0^D \sum_{i=1}^{i=N_S}\sum_{j=1,i\neq j}^{j=N_S}\delta[\mathbf{r}+\mathbf{r}_i(t)-\mathbf{r}_j(t)]\mathrm{d}t}{4\pi r^2 N_S D\,\Delta r}, & s=0 \\ \dfrac{\displaystyle\int_0^{D-s} \sum_{i=1}^{i=N_S}\sum_{j=1}^{j=N_S}\delta[\mathbf{r}+\mathbf{r}_i(t+s)-\mathbf{r}_j(t)]\mathrm{d}t}{4\pi r^2 N_S (D-s)\,\Delta r}, & s\neq 0 \end{cases} \quad (36)$$

where

$$\delta[\mathbf{x}] = \begin{cases} 1 & \text{if } |\mathbf{x}| \in [0\ \Delta r) \\ 0 & \text{otherwise} \end{cases} \quad (37)$$

δ is a probability distribution function that measures if the separation between a pair of beads lies in the spherical shell contained between radii r and $r + \Delta r$, where Δr is an infinitesimal increment in the spherical radius. Theoretically, $\Delta r \rightarrow 0$ but for simulation one needs a finite value, so, we have taken a very small value of $\Delta r = 0.02b$ where b is the ideal spring length, 1.53 Å.

The scattering function in Figure 10 is plotted against time made dimensionless using the wavenumber, q, and center-of-mass diffusivity $D_G = k_BT/\zeta_T$, where $\zeta_T \equiv (N_S + 1)\zeta$ is the drag coefficient of the whole chain. The plot has data for 60-spring chains with and without the bending and torsional potentials at a small and a large value of q, which is related to the inverse of the chain's radius of gyration. In dimensionless form, when q is increased from 5×10^8 to 3×10^9 m^{-1} with only the stretching force present, the data for both values of q collapse nearly perfectly on the same curve that is close to a single exponential decay. When bending and torsional forces are added, we observe that the relaxation of the scattering function at the smallest q value in this analysis, i.e., 5×10^8 m^{-1}, is the same as the relaxation with only stretching force present. However, at larger q value, we do see some speed-up in relaxation when bending and torsional forces are present. The similarity of these results plotted on this dimensionless time scale, and the near-exponential decay imply that the scattering function is reflecting primarily simple center of mass diffusion whose rate scales as q^2. This is precisely the behavior recorded by Ewen and Richter[35] in their Figure 43 in neutron spin–echo experiments for dilute solutions of short chains which are comparable to the chain lengths simulated here. For longer chains, at larger q, the scattering function decays more rapidly which reflects subdiffusive motion of portions of the polymer coil and is in agreement with the Zimm theory. However, for short chains such as those studied here, this subdiffusive behavior is not observable and only scaling similar to that shown in Figure 10 is seen indicating that the scattering function is not sensitive to the rotational restrictions on bond orientation that control the bond vector autocorrelation function and the mechanical stress. This is not surprising since the scattering function tracks only relative motion of mass centers which are able to diffuse collectively in space even if the bonds connecting them suffer significant restrictions on their orientational rearrangements. Hence, there is no contradiction between the dramatic changes that bending and torsional potentials induce in orientational dynamics and the rather minor effect that they have on the decay of the scattering function.

6. Conclusions

Using a locally realistic bead−spring model with stretching, bending, and torsional potentials, we show that local relaxations of small numbers of bonds—corresponding to normal modes with large mode number—are slowed greatly by the bending and torsional potentials which push the relaxation times for local modes toward the terminal region for short chains. This effect is more pronounced when the trans/gauche torsional barrier height is increased with large deviations from Rouse model predictions being observed for all but the slowest mode for chains containing up to 60 bonds.

We tested a standard coarse-graining method that replaces the locally realistic fine-grained (FG) chain constrained by bending and torsional potentials by a freely jointed coarse-grained (CG) chain. The length of each CG bond and the number of FG bonds replaced by each CG bond are chosen to achieve a match of the CG model to the FG model in the equilibrium coil size and in the fully stretched length of the chain. We find that the CG model is typically not able to capture accurately the dynamics of the FG model except at long times. Thus, coarse-graining a polymer to a freely jointed (bead−rod) chain might not always be a very successful strategy for reducing polymer degrees of freedom while preserving accuracy. In fact, data for polystyrene and polyisoprene in dilute solution show that the simple bead−spring model, with around 100 bonds subsumed into a single spring, might be a more successful coarse-grained model for describing linear viscoelasticity than is the bead-rod model.

Our results help explain why the viscoelasticity of a dilute polymer solution shows less evidence of local motion than is observed in a melt of the same polymer. The reason is the greater slowdown, in dilute solutions relative to the melt, of local motions caused by bending and torsional barriers to bond motion. In both dilute solutions and melts, slow small-k modes involving collective motion of many bonds are controlled entirely by diffusive resistance to motion which is proportional to solvent viscosity and not influenced by bending and torsional barrier heights. These slow modes therefore follow Rouse theory, which includes only viscous diffusional resistance to bead motion and ignores rotational barriers. However, in dilute solutions, local, large-k modes, which according to the Rouse theory should be very fast, are slowed down so much by bending and torsional barriers that their relaxation rates are similar to those of collective small-k modes, and hence are not distinguishable in the viscoelastic spectrum from the low-k modes. Thus, the viscoelastic spectrum resembles that of a bead−spring model with a limited number of springs.

For a melt, there is no solvent to set the diffusive time scale of the slow modes, and so this time scale must be set self-consistently by the collective motions of the chains in a “micro-environment.” This effective viscosity of the microenvironment (which sets the monomeric friction coefficient used in the Rouse theory for melts) is typically high enough that the relaxation rate of small-k collective modes is slower than that of the local high-k modes and so these high-k modes can be distinguished from the low-k modes in the viscoelastic spectrum for melts. In effect, the “viscosity” governing local bond rotations is smaller than that of the microenvironment controlling larger scale motions, so that even when slowed by rotational barriers, the local motions remain faster than the longer range relaxations in the melt. Thus, local dynamics are readily distinguished for melts at short times in the viscoelastic spectrum. For dilute solutions, these dynamics occur nearly simultaneously with more global motions and hence are not readily discernible in the viscoelastic spectrum.

Appendix 1. Code Validation

To validate the code, we compute the change in the total potential energy of the system over a small time step and compare it to the work done on the system in this time:

$$V_S|_{t+\Delta t} - V_S|_t = \sum_{i=1}^{i=N_S+1} \mathbf{F}_S^i \cdot \Delta\mathbf{r}^i \tag{38}$$

$$V_B|_{t+\Delta t} - V_B|_t = \sum_{i=1}^{i=N_S+1} \mathbf{F}_B^i \cdot \Delta\mathbf{r}^i \tag{39}$$

$$V_T|_{t+\Delta t} - V_T|_t = \sum_{i=1}^{i=N_S+1} \mathbf{F}_T^i \cdot \Delta\mathbf{r}^i \tag{40}$$

where Δt is the time step and Δr is the distance moved by the ith bead in time Δt. That is, we use the formulas for the forces derived analytically from the potentials to evaluate the right side of each of the above equations and compare this with the change in potential over a single time step calculated directly from the expression for each potential. This procedure validates not only that the formulas for the forces are correctly derived and written into the computer code but also determines the time step that is small enough to accurately calculate the change in potential. To ensure that the model is able to replicate the system accurately, we require that the spring length and bending angle remain close to the ideal values. In order to do so, we use “realistic” values of the parameters,[24] i.e., $\gamma_S/m = 1.8 \times 10^{28}$ s^{-2} and $\gamma_\theta/m = 4.2 \times 10^7$ J/kg. Since we are using an explicit integration scheme, we are forced in the above check to use very small time steps ($\Delta t \sim 10^{-21}$ s) to keep the changes in the potential small over a single time step.

Acknowledgment. We gratefully acknowledge the financial support provided by Petroleum Research Fund through grant No. ACS PRF # 45882-AC7 which partly funded this research.

References and Notes

(1) Lodge, T. P.; Miller, J. W.; Schrag, J. L. *J. Polym. Sci.: Polym. Phys. Ed.* **1982**, *20*, 1409–1425.

(2) Larson, R. G. *Macromolecules* **2004**, *37*, 5110–5114.
(3) Rouse, P. R. *J. Chem. Phys.* **1953**, *21* (7), 1272–1280.
(4) Zimm, B. H. *J. Chem. Phys.* **1956**, *24* (2), 269–278.
(5) Amelar, S.; Eastman, C. E.; Morris, R. L.; Smeltzly, M. A.; Lodge, T. P.; Meerwall, E. D. V. *Macromolecules* **1991**, *24*, 3505–3516.
(6) Brown, D.; Clarke, J. H. R. *J. Chem. Phys.* **1994**, *100* (2), 1684–1692.
(7) Baschnagel, J.; Qin, K.; Paul, W.; Binder, K. *Macromolecules* **1992**, *25*, 3117–3124.
(8) Mondello, M.; Grest, G. S.; Webb III, E. B.; Peczak, P. *J. Chem. Phys.* **1998**, *109* (2), 798–805.
(9) Paul, W.; Smith, G. D.; Yoon, D. Y. *Macromolecules* **1997**, *30*, 7772–7780.
(10) Rigby, D.; Roe, R.-J. *J. Chem. Phys.* **1987**, *87* (12), 7285–7292.
(11) Rigby, D.; Roe, R.-J. *J. Chem. Phys.* **1988**, *89* (8), 5280–5290.
(12) Lodge, A. S.; Wu, Y.-J. *Exact relaxation times and dynamic functions for dilute polymer solutions from the bead/spring model of rouse and zimm*; Presented at the Society of Rheology's Winter Meeting, Salt Lake City, Feb 1971.
(13) Peterson, S. C.; Echeverria, I.; Hahn, S. F.; Strand, D. A.; Schrag, J. L. *J. Polym. Sci.: Part B: Polym. Phys.* **2001**, *39*, 2860–2873.
(14) Tsunashima, Y. *J. Chem. Phys.* **2001**, *114* (20), 9163–9169.
(15) Fixman, M. *Faraday Discuss. Chem. Soc.* **1987**, *83*, 199–211.
(16) Fixman, M. *J. Chem. Phys.* **1978**, *69* (4), 1527–1537.
(17) Fixman, M. *J. Chem. Phys.* **1978**, *69* (4), 1538–1545.
(18) Moe, N. E.; Ediger, M. D. *Polymer* **1996**, *17* (10), 1787–1795.
(19) Symeonidis, V.; Karniadakis, G. E.; Caswell, B. *Comput. Sci. Eng.* **2005**, May/June, 39–46.
(20) Bekker, H.; Berendsen, H. J. C.; van Gunsteren, W. F. *J. Comput. Chem.* **1995**, *16* (5), 527–533.
(21) IUPAC-IUB. *Biochemistry* **1970**, *9*, 3471.
(22) Ryckaert, J. P.; Bellemans, A. *Chem. Phys. Lett.* **1975**, *30* (1), 123–125.
(23) Scott, R. A.; Scheraga, H. A. *J. Chem. Phys.* **1966**, *44* (8), 3054–3069.
(24) Helfand, E.; Wasserman, Z. R.; Weber, T. A. *Macromolecules* **1980**, *13*, 526–533.
(25) Chopra, M.; Larson, R. G. *J. Rheol.* **2002**, *46* (4), 831–862.
(26) Larson, R. G. *Mol. Phys.* **2004**, *102* (4), 341–351.
(27) Larson, R. G., *The structure and rheology of complex fluids*; Oxford University Press: New York, 1999.
(28) Flory, P. J. *Statistical mechanics of chain molecules*; Oxford University Press: New York, 1988; pp 16–26.
(29) Larson, R. G. *J. Rheol.* **2004**, *49* (1), 1–70.
(30) Doi, M.; Edwards, S. F. *The theory of polymer dynamics*; Calrendon Press: Oxford, UK, 1986.
(31) Larson, R. G. *Constitutive equations for polymer melts and solutions*; Butterworth Publishers: Stoneham, MA, 1988.
(32) Kuhn, W.; Grun, F. *J. Polym. Sci.* **1946**, *1* (3), 183–199.
(33) Krushev, S.; Paul, W.; Smith, G. D. *Macromolecules* **2002**, *35*, 4198–4203.
(34) Faller, R.; Muller-Plathe, F. *Polymer* **2002**, *43*, 621–628.
(35) Ewen, B.; Richter, D. *Adv. Polym. Sci.* **1997**, *134*, 1–129.
(36) Putz, M.; Kremer, K.; Grest, G. S. *Europhys. Lett.* **2000**, *49* (6), 735–741.
(37) Binder, K.; Kob, W. *Glassy materials and disordered solids*; World Scientific Publishing Co. Ltd.: Singapore, 2005.
(38) Allen, M. P.; Tildesley, D. J. *Computer simulation of liquids*; Oxford University Press: New York, 1987.

MA702343W